Multi-input multi-output antenna measurements with super wide bandwidth for wireless applications using isolated T stub and defected ground structure

Pradeep Vinaik Kodavanti[1], P. V. Y. Jayasree[2], Prabhakara Rao Bhima[3]

[1] *Department of Electronics and Communication Engineering, Jawaharlal Nehru Technological University Kakinada, Kakinada-533003, Andhra Pradesh, India*

[2] *Department of Electrical, Electronics and Communication Engineering, GITAM, Visakhapatnam-530045, Andhra Pradesh, India*

[3] *School of Nano technology, Jawaharlal Nehru Technological University Kakinada, Kakinada-533003, Andhra Pradesh, India*

ABSTRACT
The paper presents the idea of defective ground structures for the improvement in the radiation characteristics of the antenna especially in the multi-input multi-output (MIMO) configuration. The proposed antenna model with partially flared out feed system is designed and analyzed with defective ground in both single and array configuration. A T stub is a T shaped stub used in this work with defected ground structure. A T stub is included along with defective ground to enhance the MIMO configuration features. The simulations are carried out on electromagnetic modelling tool and analyzed by measuring the parameters like reflection coefficient, voltage standing wave ratio (VSWR), gain, radiation pattern and current distribution plots. For the fabrication of the proposed antenna these measurements are very important. The antenna is fabricated and validated in terms of S-parameters and VSWR. The proposed results are good agreement with the simulated results. The overall size of the antenna is 24 × 18 × 0.8 mm³.

Corresponding author: Pradeep Vinaik Kodavanti, e-mail: pradeepvinaik.kodavanti@gmail.com

1. INTRODUCTION

An antenna is the most significant part of the communication system which is responsible for the transmission and interception of the electromagnetic signal [1]-[10]. Several configurations like single element, array and multiple elements radiating systems are existing for efficient communication link [11]-[15]. The ultra-wide band (UWB) based systems have become the most significant part personal and commercial wireless systems. This certainly led to huge number of applications like Wi-Fi, WLAN, and Bluetooth etc. Hence it is a challenging task for the antenna engineers to design antennas with typical radiation pattern and spectrum characteristics which does not entertain the spatial or frequency interference. Hence antennas with several notch band features are the solution to such interference issues. The other significant parameter is the channel characteristics which

contribute to the power efficiency of the system. It is always a challenging task to enhance the capability of the channel without effecting its spectral and spatial response. Multi-input multi-output (MIMO) emerged as the best solution to meet the above requirements. The technology observes weak coupling between the radiating systems. However, the design challenges do persist in order to perceive the miniaturization and portability of the system. Several works have reported significant results pertaining to the UWB MIMO based designs.

Parameters like isolation and its improvement has been the most desirable design issue of MIMO UWB antennas. The isolation improvements can be achieved through the decoupling process or characteristics of the antennas. The process is inherently complex in nature [8]-[12]. Radiating system with excellent diversity is another solution to achieve the desired characteristics of MIMO with good decoupling. Incorporating the filters and other circuits are another best option for achieve

this objective of isolation. Slots, stubs, split ring resonator are some examples of structures proposed to embed with the radiating system to realize the notch bands and inference patterns [13]-[15]. Recently, several other structures which are conformal are considered as the advancements in antenna design for 5G technology [16], [17]. This technique is projected as the most favorable feature for the advanced communication. Measurement of various parameters are very important in the design, fabrication and analysis of the antenna. Section 2 describes the proposed antenna geometry with and without T stub. The simulation results are discussed in the section 3. The overall conclusion in included as section 4.

2. PROPOSED ANTENNA GEOMETRY

The proposed antenna has a typical initial geometry of patch antenna with two conducting plates sandwiched between a dielectric substrate. The conducting plate on the top side serves as the radiation source which is in circular in shape and edge fed. The bottom plate serves as ground plane which is defective in shape intentionally to represent the defective ground features.

The usual edge feed geometry is a rectangular strip running from the edge of the radiating patch to the end of the substrate. However, in this work the shape of the rectangular strip has been modified. From the edge of the substrate, the feed line takes the shape of rectangle for a length of $Lf2$ and width of Wf and flares out as it reaches the edge of the circular patch where it assumes the width of $Wf2$ which is greater than Wf. The length of the gradual flaring of the feedline is $Lf3$. The circular patch has a radius of r while the substrate has dimensions like length L and width W.

The ground plane on the other side is defective in nature and does not have s specific shape to define. It can be considered that a rectangular strip of length Lg and width similar to that of the substrate at lower edge of the substrate plane. Remaining part of the ground plane is left uncoated with ground plane conductor. The strip along the width W has three V shaped valleys. It can be considered that the two V shaped valleys on either side of the centre V shape are symmetric in nature and have the V arm

length $L1$ less than that of $L2$ which is the arm length of the central deep V shape.

The table describing the optimized dimensions of the geometry proposed for the antenna is given in Table 1 in which all the dimensions are measured in mm scale.

The geometry has been enhanced to the array configuration with two similar elements arranged side by side on the radiation region as shown in Figure 1(c). The two-element array configuration is necessary to realise the MIMO characteristics of the antenna. The ground characteristics and the geometry in the first case of is similar to the Figure 1(b) however, duplicated and copied in order to serve the defective ground of the second
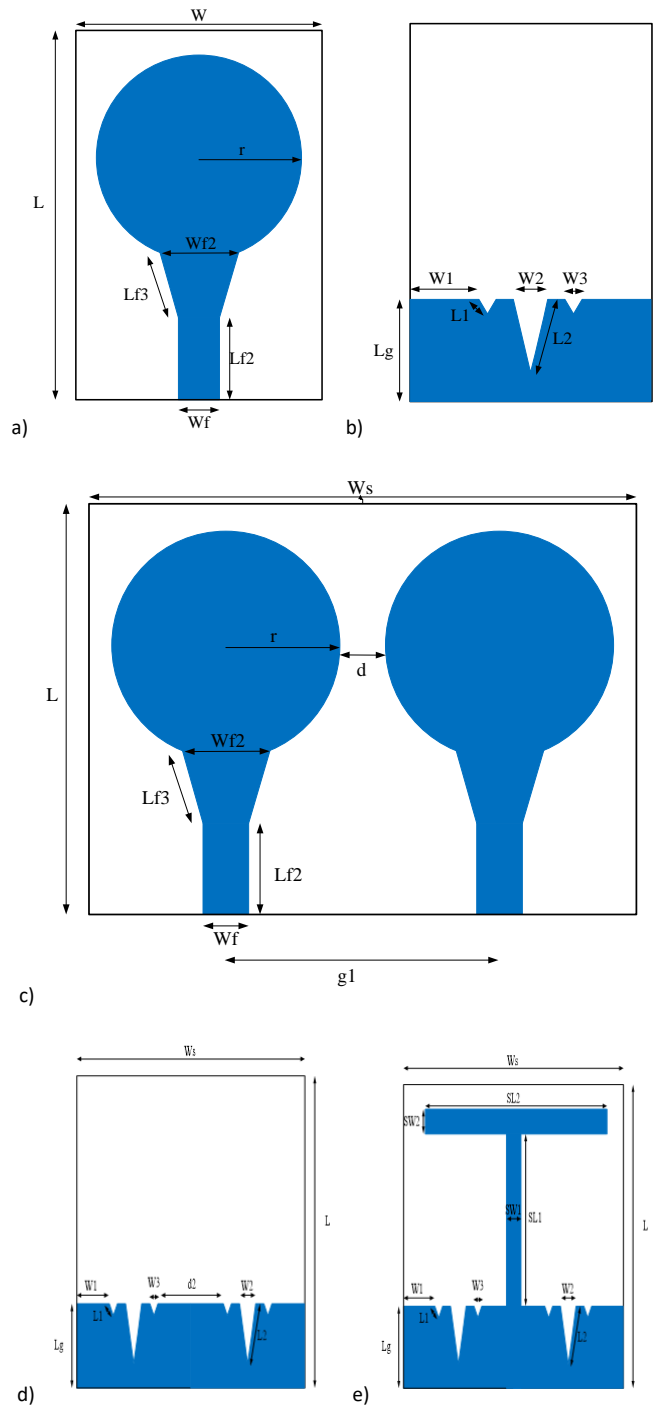

a)

b)

c)

d)

e)

Figure 1. Proposed Super Wide Band Antenna (a) Front view (b) Ground Plane and MIMO Antenna (c) Front View (d) Ground Plane without T Stub and (e) Ground with T Stub.

Table 1. Antenna Design Parameters.

S. No	Parameter	Value in mm
1	L	18
2	Ws	24
3	Wf	1.5
4	Lf	6
5	r	5.5
6	Lf1	6.5
7	Wf1	3
8	Wf2	2.5
9	Lf2	3
10	Lf3	3.39
11	Lg	6
12	L1	1
13	L2	3.8
14	W1	2.5
15	W2	3
16	W3	2
17	g1	12
18	d	1
19	d1	5
20	SL1	11
21	SL2	0.5
22	SW1	0.5
23	SW2	6
24	d2	5

element in the array. Further, the T stub is included in the second case of interest to enhance the MIMO characteristics. In this case, the T stub arises from the centre of the ground plane and specifically from the top edge of the strip for defective ground configuration. The two rectangular strips are arranged perpendicular to each other to form the T shape. The vertical strip has dimensions of SL1 length and *SW1* width while the dimensions of the horizontal strip is *SL2* and *SW2*.

3. RESULTS AND DISCUSSION

The radiation characteristics of the simulated antenna using the EM modelling tool are presented in this Section as follows. The results are presented as three cases in which the first case refers to the proposed antenna in its single element form with defective ground. The second case refers to the two-element array configuration and the third case is the MIMO antenna with the T stub in the defective ground.

3.1. Case-1: Defective Ground Antenna

The frequency response and the resonance features can be directly inferred from the *S11* plot as presented in Figure 2(a). The same can be validated or verified using the corresponding voltage standing wave ratio (VSWR) plot given in Figure 2(b). Further, the frequency dependant gain characteristics are studied using the Gain plot in Figure 2(c).

From the *S11* and VSWR plot, it is evident that the antenna designed has a very large band starting from 6 GHz covering almost to the frequencies above 80 GHz with a continuous consistency in reflection coefficient less than -10dB. Within the range it is possible to find several dips in the response curve
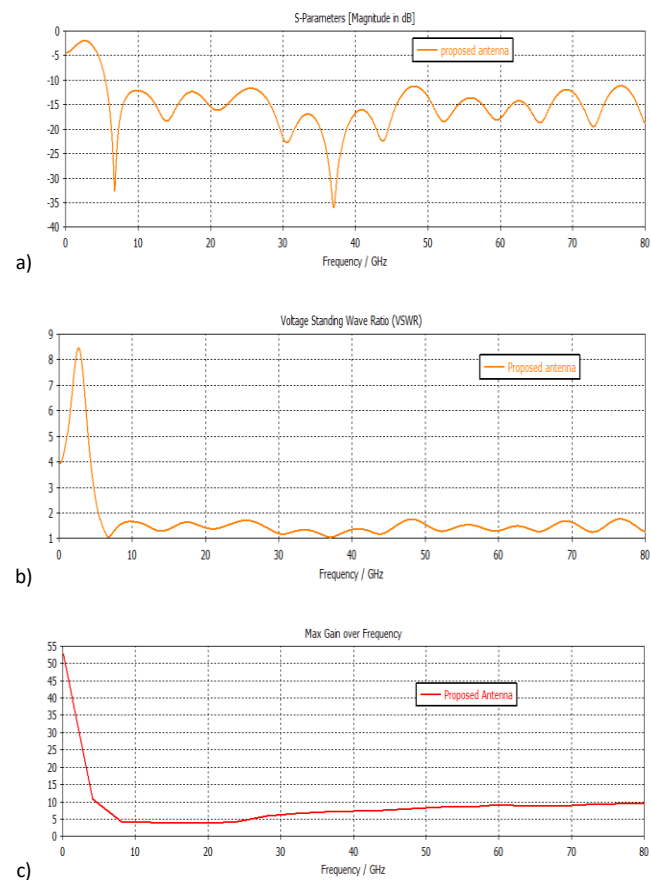

Figure 2. Proposed SWB Antenna simulation Results (a) S11 (b) VSWR and (c) Maximum Gain versus Frequency.
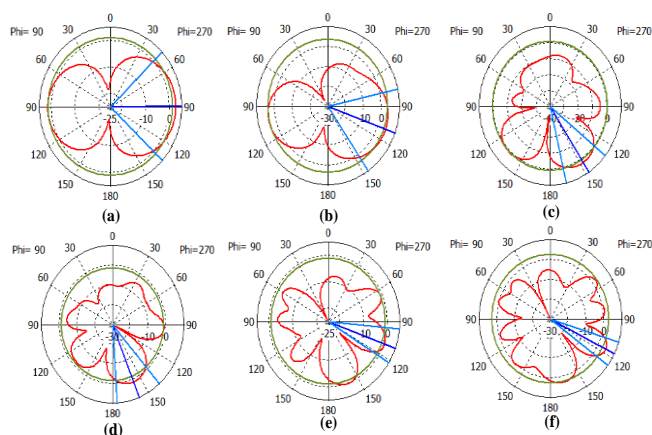

Figure 3. Simulation Radiation patterns of proposed antenna at (a) 6.73 GHz, (b) 13.92 GHz, (c) 30.54 GHz, (d) 37.01 GHz, (e) 43.8 GHz and (f) 52.2 GHz.

where the corresponding characteristics are highly resonant. Similarly, the VSWR magnitude is below 2 through the entire sweep as mentioned above for *S11*. This confirms the radiation characteristics once again.

Similarly, from the gain plot it is possible to mention that the maximum gain is continuously increasing form the lower side of the resonant band to the upper side. Initially, the max gain takes a linear decrement from the 5 GHz to 8 GHz while after that a gradual but very slow enhancement is observed till 80 GHz.

Further, the *S11* and VSWR are frequency response curves while the consistency in the radiation characteristics cannot be inferred from the radiation pattern plots which are presented for various frequencies presented in Figure 3(a) through Figure 3(f). The frequencies of interest are the dips observed in the S11 pot where there is maximum reflection coefficient for the antenna. In this work, the polar radiation characteristics plots are presented for 6.73 GHz, 13.92 GHz, 30.54 GHz, 37.01 GHz, 43.8 GHz and 52.2 GHz.

The radiation characteristics are very much close the template patterns of a patch antenna and also the have similarity. Further, the radiation pattern is highly dependent on the current distribution which is again defined by the geometrical conditions of the antenna and the feed point orientation and construction. In order to study the same, the current distribution is given in
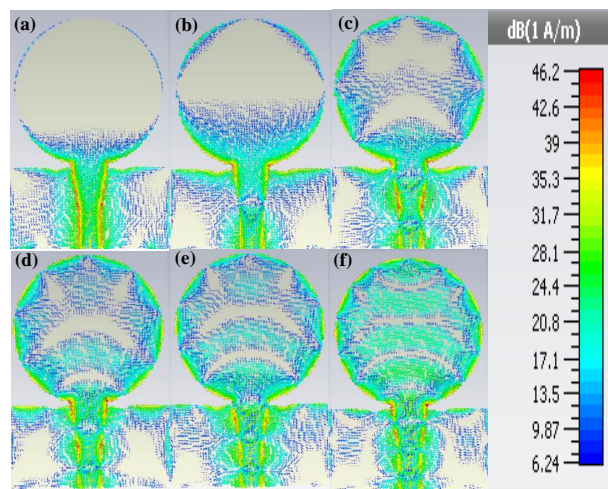

Figure 4. Simulation Current Distributions of proposed antenna at (a) 6.73 GHz, (b) 13.92 GHz, (c) 30.54 GHz, (d) 37.01 GHz, (e) 43.8 GHz and (f) 52.2 GHz.
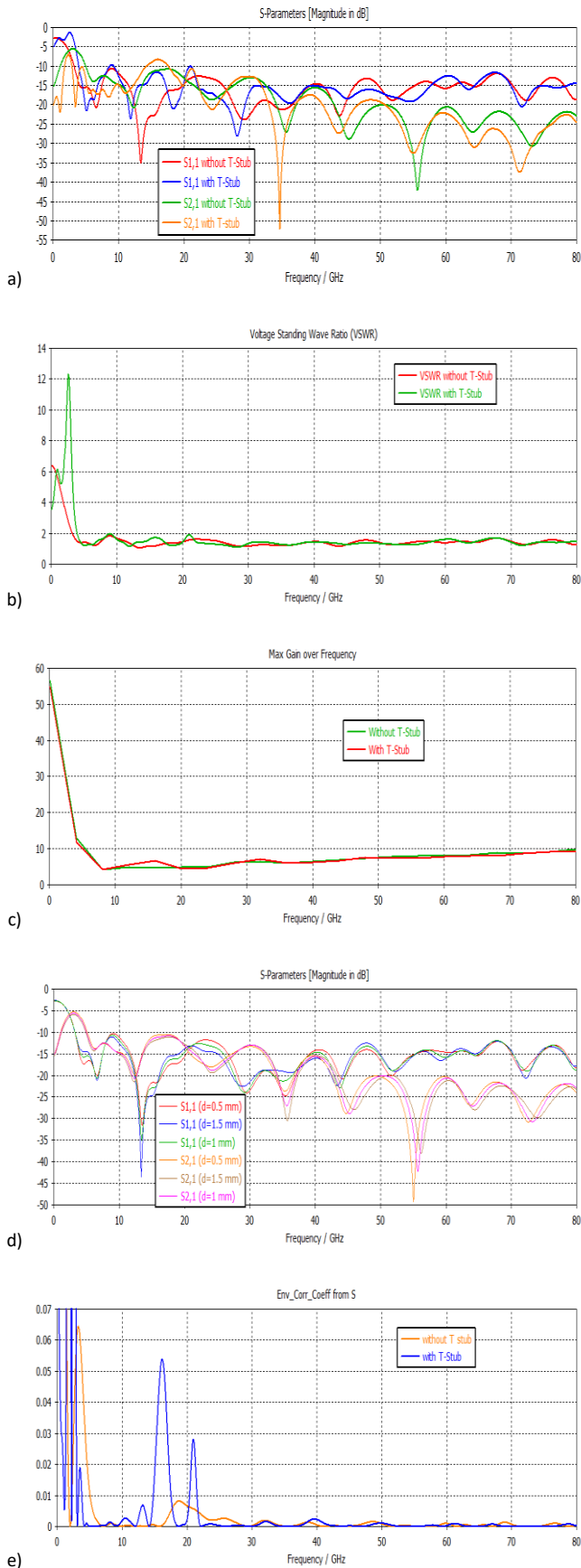
a)

b)

c)

d)

e)

Figure 5. Simulation Results of Proposed MIMO Antenna (a) S11 (b) VSWR (C) Gain Versus Frequency (d) varying distance (d) between two circular patches with a step size of 0.5 mm and (e) Envelope Correlation Coefficient (ECC).

Figure 4(a) through Figure 4(f) for the same frequencies of interest for which the radiation patterns are plotted.

In the first three figures, the upper portion of the patch geometry has almost no current distributed and hence the null patterns are visible in the radiation characteristics presented in Figure 3. Further, at higher frequencies, the current distribution initiated and hence the expansion of the beams is visible in patterns slowly dominating the null characteristics.

3.2. Case-2: Two element array configuration

The two-element array configuration of the defective ground antenna is studied in terms of its resonant features from the plotted $S11$ and VSWR graphs in Figure 5(a) and Figure 5(b). The array $S11$ plot is much like that of the single element without any deviation in its resonant features. This is a favourable case for the array configuration as the we do not want the resonant characteristics of the antenna to be disrupted in the array form. Similarly, the transmission characteristics from first port to the second port can be studied from the $S21$ plot which is also plotted in the same figure. The $S21$ features the same characteristics expect the case of variation in the magnitudes. This is evident in the graph of $S21$.

In order to convince the $S11$ characteristics, the corresponding VSWR features are plotted in Figure 5 (b) which exhibit the same resonance of the antenna with the corresponding magnitude of the parameter keeping below 2 for the entire range of the frequency band starting from 5 GHz to 80 GHz.

In the gain plot presented in Figure 5 (c) and observed to better than the maximum gain observed from Figure 2 (c). The $S11$ of proposed antenna by varying distance (d) between two circular patches with a step size of 0.5 mm is represented in Figure 5(d). Further, the envelope correlation has been computed for and presented to correlate the envelope features of the characteristics as shown in Figure 5 (e). The correlation is denied in the non-resonant band while was excellent in the resonant band of the antenna.

Similarly, the current distribution is plotted for the array configuration without the T stub and presented in Figure 6(a) through Figure 6(f) following this also have the radiation polar plots of the array configuration without stub in Figure 7(a) through Figure 7(f). It is possible to correlate both the current distribution and the polar radiation plots as the current distribution greatly effects the radiation characteristics. The null patterns are completely defined by the no current distribution zones on the surface of the radiating area of the antenna.
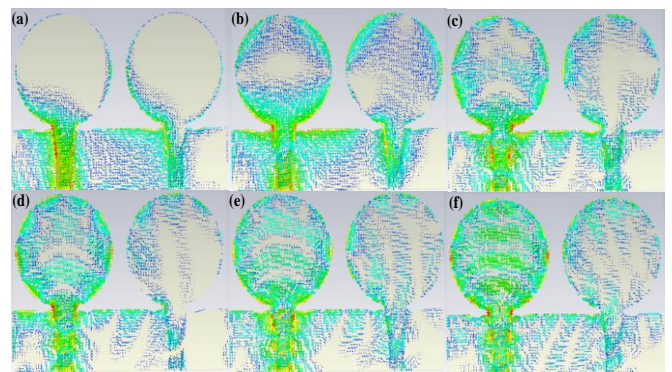

Figure 6. Simulation Current Distributions of proposed MIMO antenna without T Stubs at (a) 6.73 GHz, (b) 13.92 GHz, (c) 30.54 GHz, (d) 37.01 GHz, (e) 43.8 GHz and (f) 52.2 GHz.
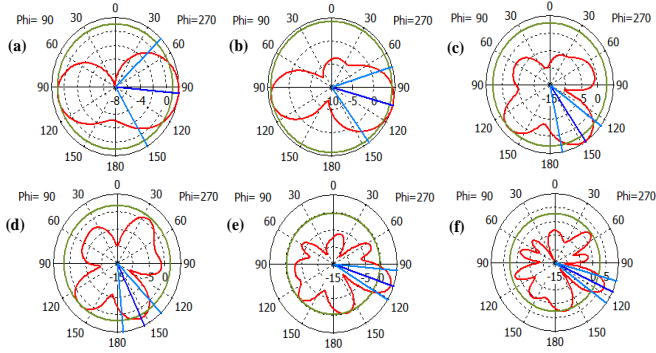
Figure 7. Simulation Radiation Patterns of proposed MIMO antenna without T Stubs at (a) 6.73 GHz, (b) 13.92 GHz, (c) 30.54 GHz, (d) 37.01 GHz, (e) 43.8 GHz and (f) 52.2 GHz.

Figure 9. Simulation Radiation Patterns of proposed MIMO antenna with T Stubs at (a) 6.73 GHz, (b) 13.92 GHz, (c) 30.54 GHz, (d) 37.01 GHz (e) 43.8 GHz and (f) 52.2 GHz.

3.3. Case-3: Array Antenna with T stub

The array configuration with T Stub is as shown in Figure 2(e). The $S11$, $S21$ and the VSWR plots are given in Figure 5(a) through Figure 5(b). The inclusion of the T stub has no appreciable impact on the S11 plot while the $S21$ produced a notch band around the 15 GHz frequencies. Similarly, the VSWR plots have the same features as that of the S11. The gain consideration as relatively unaltered due to the T stub as shown in Figure 5(c) and the ECC observes a shift in the band at the initial stage which however has no impact as it is outside the band of operation as shown in Figure 5(d).

The current distribution and the radiation characteristics are presented in Figure 8 and Figure 9 respectively for the array without T stub model. Both the plots are highly correlated with the radiation pattern defined by the corresponding current distribution. The plane in which the current distribution is maximum observes main beam orientation in the radiation pattern. Similarly, the no current zone accommodates the wide nulls in the plane of radiation. At 52.2 GHz, the first element has the maximum current on its surface and the corresponding pattern observes maximum radiation from azimuthal 120^0 to 180^0. So as the case with all the remaining.

The fabricated prototype of the proposed antenna is represented in Figure 10. The measured and simulated result comparison of S-parameters and VSWR of proposed antenna is represented in Figure 11 and Figure 12. The measured results are good agreement with the simulated results and is applicable for real time applications.

Figure 10. Fabrication prototype of proposed antenna.

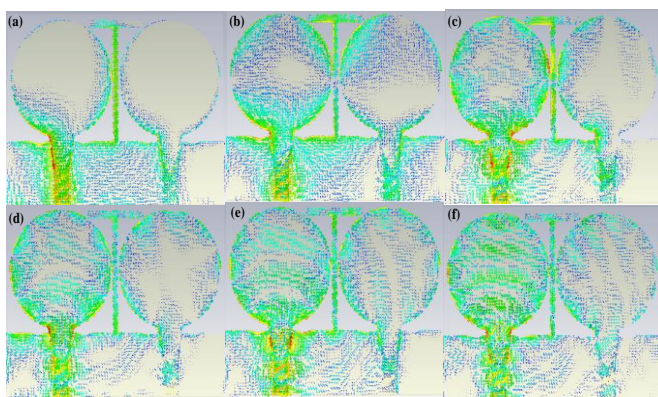Figure 11. Simulated and Measured S11 and S12 for the proposed antenna.

Figure 8. Simulation Current Distributions of proposed MIMO antenna with T Stubs at (a) 6.73 GHz, (b) 13.92 GHz, (c) 30.54 GHz, (d) 37.01 GHz, (e) 43.8 GHz and (f) 52.2 GHz.
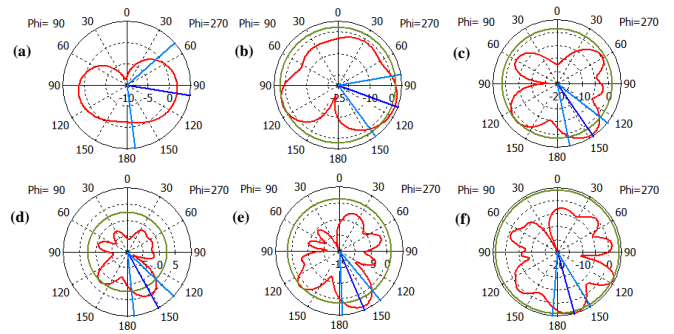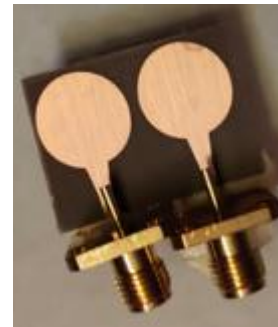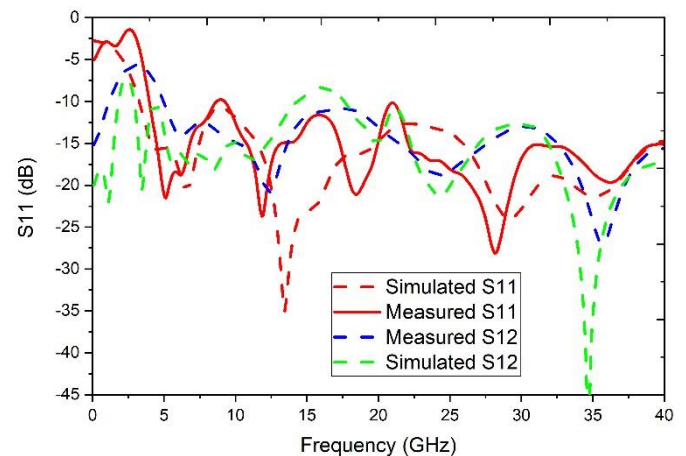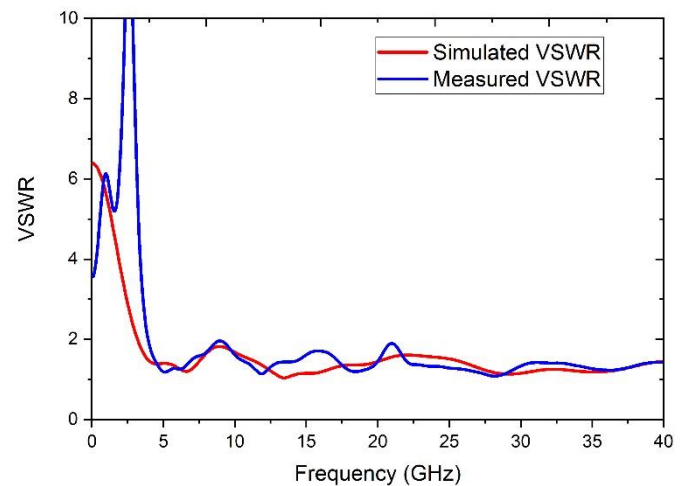

Figure 12. Simulated and Measured VSWR for the proposed antenna.

Table 2. Comparing proposed antenna with previous literature.

Ref	Size (mm³)	Substrate	Band Width (GHz)	Gain (dB)	ECC
[18]	48 × 48 × 0.8	FR4	2.5 - 12	NA	< 0.005
[19]	50 × 50 × 1.6	RO-6035HTC	2.76 - 10.75	2.5 - 5	< 0.025
[20]	23 × 26 × 0.8	FR4	3.1 - 10.6	2 - 4.5	< 0.01
[21]	50 × 39.8 × 1.524	RO-TMM4	2.7 - 12	2.5 - 6.0	< 0.01
[22]	60 × 120 × 1.5	RO-4350	0.75 - 7.65	3.2	< 0.1
[23]	58 × 58 × 1	FR4	2.9 - 40	4.3 - 13.5	< 0.04
proposed	18 × 24 × 0.8	Rogers 5880	5.5 - 80	4.01 - 9.89	< 0.05

The proposed antenna is compared with previous literature in terms of different parameters of Size, substrate, bandwidth, Gain and ECC are tabulated in Table 2. The ECC is a dimension less quantity.

4. CONCLUSION

The planar microstrip antenna-based structure using defective ground with T stub has been successfully simulated and analysed for its SWB and MIMO characteristics. A clear improvement in terms of the antenna radiation properties is evident from the single and two element array configurations of the MIMO antenna. The presence of the T Stub has relevance to the notch band characteristics of the antenna. Fabrication and prototyping of the antenna have a good scope to validate the results further in a practical environment.

REFERENCES

[1] Zeeshan Ahmed, Gul Perwasha, Ultrawide band antenna with wlan band-notch characteristic, Int. Conf. Comput., control commun (2013), pp. 25–26.
DOI: 10.1109/IC4.2013.6653762

[2] Noman Waheed, Abubakar Saadat, Ultra-wide band antenna with wlan and wimax band-notch characteristic, Int Conf Commun, Comput Digital syst 8 (2017).
DOI: 10.1109/C-CODE.2017.7918910

[3] Z. Q. Li, C. L. Ruan, A small integrated bluetooth and uwb antenna with wlan bandnotched characteristics, Int. Symp. Signals, Syst Electron 1 (2010), pp. 1–4.
DOI: 10.1109/ISSSE.2010.5638206

[4] Bo-Ren Hsiao, Yi-An Chen, LTE MIMO Antennas on variable sized Tablet computers with comprehensive Band coverage, IEEE Antennas Wirel. Propag. Lett. 15 (2015), pp. 1152–1155.
DOI: 10.1109/LAWP.2015.2496966

[5] Saber Soltani, Parisa Lotfi, A port and frequency reconfigurable MIMO slot antenna for WLAN applications, IEEE Trans. Antennas Propag. 64 (4) (2016), pp. 1209–1217.
DOI: 10.1109/TAP.2016.2522470

[6] Manoj K. Meshram, A novel quad-band diversity antenna for LTE and wi-fi applications with high isolation", IEEE Trans. Antennas Propag. 60 (9) (2012), pp. 4360–4371.
DOI: 10.1109/TAP.2012.2207044

[7] Shrivishal Tripathi, Akhilesh Mohan, Sandeep Yadav, A compact koch fractal UWB MIMO antenna with WLAN band-rejection, IEEE Antennas Wirel. Propag. Lett. 14 (2015), pp. 1565–1568.
DOI: 10.1109/LAWP.2015.2412659

[8] Muhammad Saeed Khan, Ultra-compact dual polarized UWB MIMO antenna with meandered feeding Lines, IET Microw., Antennas Propag. 11 (7) (2017), pp. 997–1002.
DOI: 10.1049/iet-map.2016.1074

[9] Mohammad Abedian, Compact ultrawide band MIMO dielectric resonator antennas with WLAN band rejection, IET Microw., Antennas Propag. 11 (11) (2017), pp. 1524–1529.
DOI: 10.1049/iet-map.2016.0299

[10] Mohammad Mahdi Farahani, Mutual coupling reduction in millimeter-wave MIMO antenna array using a meta material polarization-rotator wall, IEEE Antennas Wirel. Propag. Lett. 16 (2017), pp. 2324–2327.
DOI: 10.1109/LAWP.2017.2717404

[11] Mohammad Saeed Khan, A compact CSRR-enabled UWB diversity antenna, IEEE Antennas Wirel. Propag. Lett. 16 (2017), pp. 808–812.
DOI: 10.1109/LAWP.2016.2604843

[12] Wing-Xin Chu, Compact broad band slot MIMO antenna with a stub loaded radiator, IEEE conference on Antenna Measurements and Applications (2014), pp. 1–4.
DOI: 10.1109/CAMA.2014.7003407

[13] V. Jyothika, M. S. P. C. Shekar, S. V. Krishna, M. Z. U. Rahman, Design of 16 element rectangular patch antenna array for 5g applications, Journal of Critical Reviews, 7 (9) (2020), pp. 53-58.

[14] V. S. Chakravarthy, P. M. Rao, Amplitude-only null positioning in circular arrays using genetic algorithm. IEEE International Conference on Electrical, Computer and Communication Technologies (ICECCT), pp. 1-5.
DOI: 10.1109/ICECCT.2015.7226120

[15] K. Aravind Rao, K. Sai Raj, R. K. Jain, M. Z. U. Rahman, Implementation of adaptive beam steering for phased array antennas using enlms algorithm, Journal of Critical Reviews, 7 (9) (2020), pp. 59-63.
DOI: 10.31838/jcr.07.09.10

[16] S. Blanch, J. Romeu, Exact representation of antenna system diversity performance from input parameter description, Electron. Lett. 39 (9) (2003), pp. 705–707.
DOI: 10.1049/el:20030495

[17] H. Huang, X. Li, Y. Liu, A low-profile, dual-polarized patch antenna for 5g mimo application, IEEE Trans. Antennas Propag. 67 (2) (2019), pp. 1275–1279.
DOI: 10.1109/TAP.2018.2880098

[18] S. Kesana, S. Gatikanti, M. Z. Ur Rahman, B. Radhika, D. Mounika, Triple frequency G-shape MIMO antenna for wireless applications, International Journal of Engineering and Advanced Technology, 8 (5) (2019), pp. 942-947.

[19] Armando Coccia, Federica Amitrano, Leandro Donisi, Giuseppe Cesarelli, Gaetano Pagano, Mario Cesarelli, Giovanni D'Addio, Design and validation of an e-textile-based wearable system for remote health monitoring, Acta IMEKO, vol.10, 2021, no.2, pp. 1-10.
DOI: 10.21014/acta_imeko.v10i2.912

[20] H. T. Chattha, F. Latif, F. A. Tahir, M. U. Khan, X. Yang, Small-sized UWB MIMO antenna with band rejection capability, IEEE Access, 7 (2019), pp. 121816–121824.
DOI: 10.1109/ACCESS.2019.2937322

[21] S. V. Devika, K. Karki, S. K. Kotamraju, K. C. Sri Kavya, M. Z. U. Rahman, A new computation method for pointing accuracy of cassegrain antenna in satellite communication, Journal of Theoretical and Applied Information Technology, 95 (13) (2017), pp. 3062-3074.

[22] R. Hussain, M. S. Sharawi, A. Shamim, An integrated four-element slot-based MIMO and a UWB sensing antenna system for CR platforms, IEEE Trans. Antennas Propag., 66 (2) (2018), pp. 978–983.
DOI: 10.1109/TAP.2017.2781220

[23] C. Yu, S. Yang, Y. Chen, W. Wang, L. Zhang, B. Li, L. Wang, A Super-Wideband and High Isolation MIMO Antenna System Using a Windmill-Shaped Decoupling Structure, *IEEE Access*, 8 (2020), pp. 115767-115777.
DOI: 10.1109/ACCESS.2020.3004396